Neurogranin Controls the Spatiotemporal Pattern of Postsynaptic Ca^{2+}/CaM Signaling

Yoshihisa Kubota,* John A. Putkey,† and M. Neal Waxham*
*Department of Neurobiology and Anatomy, and †Department of Biochemistry and Molecular Biology, University of Texas Medical School, Houston, Texas

ABSTRACT Neurogranin (Ng) is a postsynaptic IQ-motif containing protein that accelerates Ca^{2+} dissociation from calmodulin (CaM), a key regulator of long-term potentiation and long-term depression in CA1 pyramidal neurons. The exact physiological role of Ng, however, remains controversial. Two genetic knockout studies of Ng showed opposite outcomes in terms of the induction of synaptic plasticity. To understand its function, we test the hypothesis that Ng could regulate the spatial range of action of Ca^{2+}/CaM based on its ability to accelerate the dissociation of Ca^{2+} from CaM. Using a mathematical model constructed on the known biochemistry of Ng, we calculate the cycle time that CaM molecules alternate between the fully Ca^{2+} saturated state and the Ca^{2+} unbound state. We then use these results and include diffusion of CaM to illustrate the impact that Ng has on modulating the spatial profile of Ca^{2+}-saturated CaM within a model spine compartment. Finally, the first-passage time of CaM to transition from the Ca^{2+}-free state to the Ca^{2+}-saturated state was calculated with or without Ng present. These analyses suggest that Ng regulates the encounter rate between Ca^{2+} saturated CaM and its downstream targets during postsynaptic Ca^{2+} transients.

INTRODUCTION

In the excitatory synapse of hippocampal CA1 pyramidal neurons, the activation of calmodulin (CaM)-dependent enzymes during elevations of intracellular Ca^{2+} results in the induction of synaptic plasticity, e.g., long-term potentiation (LTP) and long-term depression (LTD). Importantly, both the induction of LTP and the induction of LTD require increased Ca^{2+}, activation of CaM and activation of CaM-dependent enzymes (1). Calmodulin's critical role in plasticity was shown experimentally where direct injection of Ca^{2+} and CaM together, but not Ca^{2+} or CaM independently, into postsynaptic CA1 pyramidal neurons produced synaptic strengthening similar to LTP (2). This and many other studies using various pharmacological approaches identify CaM as a critical mediator in the processes of both LTP and LTD induction (3). Such studies make it clear that the access of Ca^{2+}-saturated CaM to its specific target must be tightly regulated and is dependent upon the frequency, amplitude, timing, and spatial profile of the Ca^{2+} transient.

Calmodulin is a small, 148-amino-acid, dumbbell-shaped protein that contains four Ca^{2+}-binding sites with two sites resident in each lobe of the dumbbell (4). The two Ca^{2+} ions bind in a cooperative fashion to each lobe of CaM and the kinetics of the interactions are well defined in vitro. The on- and off-rates for Ca^{2+} binding to the N-terminal lobe of CaM are relatively fast, 500 $\mu M^{-1}\ s^{-1}$ and 2000 s^{-1}, while those in the C-terminal lobe are slower, 21 $\mu M^{-1}\ s^{-1}$ and 8.5 s^{-1}, respectively (5,6). As such, Ca^{2+} binding to the C-terminal lobe is the rate-limiting step for CaM to achieve a fully Ca^{2+} saturated state and becomes the rate-limiting step in the activation of Ca^{2+}/CaM-dependent enzymes. Therefore, proteins that can modulate Ca^{2+} binding to the C-terminal lobe are critical in determining the probability of CaM achieving a fully activated state.

Neurogranin (Ng) and PEP-19 are two such proteins and their effects on the binding kinetics of Ca^{2+} interactions with CaM were recently identified (5,7). Both of these proteins are members of the IQ motif family of CaM-binding proteins that interact with both apo-CaM and Ca^{2+}/CaM. Both appear to specifically affect Ca^{2+} binding to the C-terminal lobe of CaM, with no apparent effect on Ca^{2+} binding to the N-terminal lobe. Ng is a 78-amino-acid protein expressed exclusively in neurons and is highly enriched in pyramidal cells ($\sim$60 μM) (8). Historically, this protein was thought to function as a CaM buffer releasing CaM upon Ca^{2+} stimulation (9). Such a functionality of Ng may well play a significant role in the postsynaptic Ca^{2+} signaling pathway responsible for regulating synaptic plasticity.

A role for Ng in regulating synaptic plasticity appears clear, however, the results from two genetic knockout studies in mice (8,10) showed opposite outcomes. One study (8) showed a deficit in high-frequency-induced LTP and enhanced LTD by low-frequency stimuli, while the other knockout mice (10) showed enhanced LTP and deficits in LTD induction. In both knockout mice, the CaM-binding domain and PKC phosphorylation site of Ng were deleted (8,10). From such studies, it is safe to conclude that we do not have a clear understanding of Ng's role in the regulation of synaptic plasticity and that additional experimental work is required to establish a consolidated working model for this important protein's function.

In this article, we explore how the known biochemical properties of Ng result in regulating the spatiotemporal pattern of Ca^{2+}/CaM action in postsynaptic spines. As noted,

Submitted February 22, 2007, and accepted for publication August 2, 2007.
Address reprint requests to Y. Kubota, E-mail: Yoshihisa.Kubota@uth.tmc.edu.
Editor: Arthur Sherman.

0006-3495/07/12/3848/12 $2.00
doi: 10.1529/biophysj.107.106849

Ng interacts with Ca^{2+}/CaM and accelerates Ca^{2+} dissociation from the C-terminal lobe of CaM (5,6). By increasing the Ca^{2+} dissociation rate, Ng may regulate the length of time that CaM molecules spend in partially Ca^{2+} bound and inactive states. In other words, Ng may control the mean cycle time of Ca^{2+}/CaM: the mean time for a CaM molecule to transit from one instance of the fully Ca^{2+} saturated state to the next. In this definition, the time spent in all other states determines the length of time between the two consecutive fully Ca^{2+} saturated states. A longer mean-cycle time would result in a smaller probability of a single CaM molecule colliding with its target in an active state during a given Ca^{2+} transient. In addition, Ng may also control the first passage time defined as the transition period required for each CaM molecule to go from the apo- to the fully Ca^{2+}-saturated state.

Here we use a simple but realistic mathematical model constructed on experimental data of Ca^{2+}-CaM-Ng interactions and investigate kinetic mechanisms through which Ng regulates the mean cycle time and first passage time of Ca^{2+}/CaM. In the first section of the Results and in Methods, we explain the mathematical model of Ng-CaM interaction and the computational strategy of calculating the cycle time and the passage time at the single molecule level. In the remainder of the Results, we use the model to dissect the kinetic mechanism through which Ng controls the mean cycle time and the first passage time. Our analysis indicates that Ng increases the mean cycle time and first passage time of CaM to enter the fully Ca^{2+} saturated state through its interaction with the C-domain of CaM. We show three-dimensional (3D) single particle trajectories of a CaM molecule alternating between the fully Ca^{2+} saturated and partially Ca^{2+} saturated states to illustrate the impact of mean cycle time on the spatiotemporal range of action of Ca^{2+}/CaM. In addition, the lifetime of CaM once entering the fully Ca^{2+} saturated state was discovered to be dictated solely by the dissociation kinetics of Ca^{2+} from the N-domain of CaM.

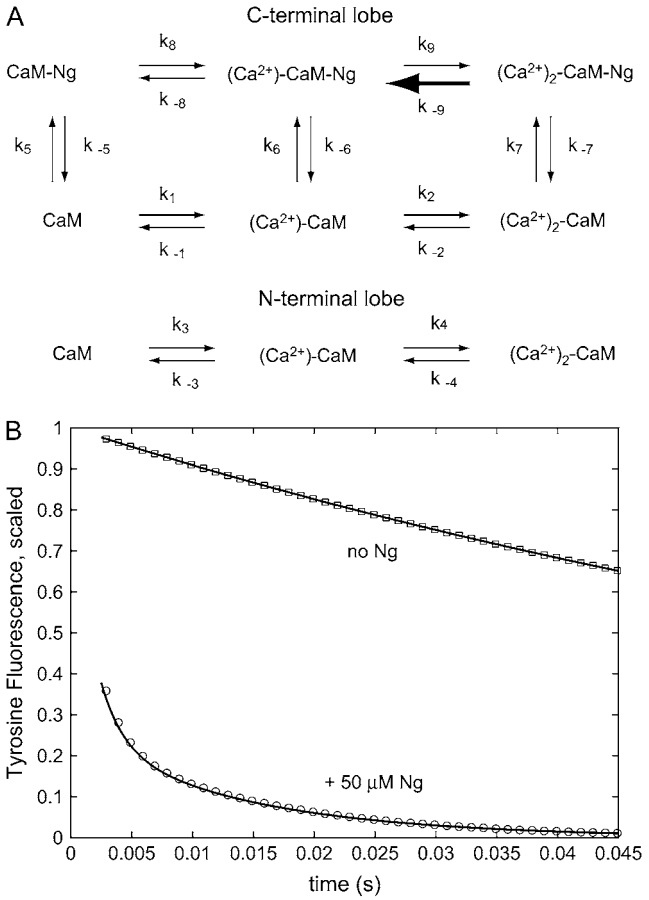

FIGURE 1 The reaction scheme of the Ng-CaM interactions and the ODE model. (*A*) A kinetic diagram showing the interactions between Ng and the C-terminal lobe of CaM. Each lobe of CaM binds two Ca^{2+} ions (*horizontal arrows*). Ng accelerates Ca^{2+} dissociation from the C-terminal lobe (*thick horizontal arrow*). Each arrow in the figure is marked by symbols, k_1, k_{-1}, k_2, k_{-2}, k_3, k_{-3}, k_4, k_{-4}, k_5, k_{-5}, k_6, k_{-6}, k_7, k_{-7}, k_8, k_{-8}, k_9, and k_{-9}, which we also use to indicate the corresponding reaction rate. The positive number subscript indicates a binding reaction while the negative number subscript is for a dissociation reaction (Table 1). The units of reaction rates are μM^{-1} s^{-1} for association rates and s^{-1} for dissociation rates. Note Ca^{2+} dissociation rate (k_{-9}) is higher than the dissociation rate (k_{-7}) of Ng from CaM (Table 1). There is presently no experimental result indicating that Ng binds to or affects Ca^{2+}-binding in the N-lobe of CaM. Therefore, we assume no binding of Ng to the N-terminal lobe (i.e., no vertical arrows). (*B*) Parameter optimization of Ng. The experimental data shown (5) was accomplished by rapidly mixing CaM (2 μM) and Ca^{2+} (100 μM) with (*solid circles*) or without (*solid squares*) 50 μM of Ng, with 5 mM EGTA and the Tyr fluorescence signal from CaM was measured as an indication of Ca^{2+} dissociation specifically from the C-terminal lobe. Thick solid lines are simulations (the ODE model) using the parameter values shown in Table 1.

METHODS

The model

Ca^{2+}, CaM, and Ng are modeled by a kinetic scheme illustrated in Fig. 1 *A*. Each lobe of CaM binds either one or two Ca^{2+} ions. Ng changes CaM's affinity toward Ca^{2+} while interacting with the C-terminal lobe of CaM and we have included the experimentally determined rate constants in the model. In other words, CaM, when in a complex with Ng, dissociates Ca^{2+} at rates different from its free form (*top rows* in Fig. 1 *A*). Thus, each CaM molecules undergoes transitions between 18 (6×3) activation states involving association and dissociation of Ca^{2+} and Ng (six different states for the C-terminal lobe and 3 for N-lobe). We first constructed an ordinary differential equation (ODE)-type model based on this kinetic scheme and the parameter values were optimized for experimental data (Fig. 1 *B*). Since Ng did not change the Ca^{2+} association rates (5), we were left with three unknown parameters (k_{-8}, k_{-9}, and k_6). The rate k_{-6} was calculated from microscopic reversibility. See Table 1 and Estimation of Reaction Rate Constants below for the optimization procedure.

The modified Gillespie algorithm and the cycle time calculations

We adopted the Gillespie-type stochastic algorithm (11) to model transitions between all possible internal states of each individual CaM molecule (or CaM-Ng complex) based on the same kinetic scheme shown in Fig. 1 and parameter values shown in Table 1. The resultant model generates the same time evolution as the ODE model (see Fig. 2). Suppose we model a binary association reaction $A+B \xrightarrow{k} C$ with a rate constant k. The propensity of

TABLE 1 Parameters used in the model (wild-type Ng)

Parameter	Symbol*	Value	Units
(C-lobe of CaM)			
Ca^{2+} binding to CaM	k_1	426	$\mu M^{-1}\ s^{-1}$
	k_2	21	$\mu M^{-1}\ s^{-1}$
Ca^{2+} binding to CaM-Ng	k_8	426	$\mu M^{-1}\ s^{-1}$
	k_9	21.5	$\mu M^{-1}\ s^{-1}$
Ca^{2+} dissociation from CaM	k_{-1}	5115	s^{-1}
	k_{-2}	8.5	s^{-1}
Ca^{2+} dissociation from CaM-Ng	k_{-8}	5830	s^{-1}
	k_{-9}	418	s^{-1}
Ng binding to apo-CaM	k_5	28	$\mu M^{-1}\ s^{-1}$
Ng binding to (Ca^{2+})-CaM	k_6	23	$\mu M^{-1}\ s^{-1}$
Ng binding to (Ca^{2+})$_2$-CaM	k_7	2	$\mu M^{-1}\ s^{-1}$
Ng dissociation from apo-CaM	k_{-5}	36	s^{-1}
Ng dissociation from (Ca^{2+})-CaM	k_{-6}	35	s^{-1}
Ng dissociation from (Ca^{2+})$_2$-CaM	k_{-7}	136	s^{-1}
(N-lobe of CaM)			
Ca^{2+} binding to CaM	k_3	500	$\mu M^{-1}\ s^{-1}$
	k_4	500	$\mu M^{-1}\ s^{-1}$
Ca^{2+} dissociation from CaM	k_{-3}	16,000	s^{-1}
	k_{-4}	2000	s^{-1}

The kinetic rates for the mutant Ng values are indicated in Fig. 5 (*insets*).
*The symbol for each kinetic rate is indicated in Fig. 1 *A*.

this reaction, defined in a conventional Gillespie scheme, is proportional to the product of the current number of A and B molecules and the reaction probability determined from the macroscopic reaction rate k. The Gillespie algorithm assumes a Poisson (exponential) distribution of the next expected reaction time for this chemical process (11). If there are other types of chemical reactions, we calculate the propensity function for those reactions and take the sum of all the propensity functions to calculate the next reaction time step. Which reaction will happen is determined according to the propensity of each chemical reaction in the system: the higher the propensity, the more likely the reaction is selected. In fact, the Gillespie algorithm or its equivalent, the Bortz-Kalos-Lebowitz (12) algorithm, relies on the fact that the sum of multiple independent Poisson processes becomes one big Poisson process (13).

We apply this principle to model the individual CaM molecules. The rationale is as follows. In the above example of binary association reactions $A+B \xrightarrow{k} C$, suppose we have n-molecules of A (say A_1 to A_n) and m-molecules of B. Instead of calculating the total propensity function of this reaction, we can calculate the propensity function for each A_i molecule ($i = 1,\ldots,n$) and carry out the Gillespie algorithm as usual. In this particular example, each A_i molecule becomes a C_i molecule if they react with one of the B molecules. One can think of this reaction as a change of the state of the i^{th} molecule (from state A to C) with a probability proportional to the product of the reaction rate k and the number of B molecules. As stated, the resultant algorithm is identical to the original Gillespie scheme but this way we can keep track of each individual A molecule in the system as they react with B molecules. In our algorithm, we calculate individual propensity functions of each CaM molecule, take a sum of all of these propensity functions, and execute Monte Carlo simulations as in the original Gillespie algorithm. This extended Gillespie-type scheme is as exact as the original Gillespie algorithm. We represent the states of CaM molecules in the simulation by an $18 \times n$ matrix whose elements are 0 or 1 where n is the total number of CaM molecules in the system and each CaM molecules has 18 different internal states. For example, if the i^{th} row of the j^{th} column of the matrix is 1, it indicates that the j^{th} CaM molecule ($j = 1,\ldots,n$) is in the i^{th} activation state ($i = 1,\ldots,18$) and the rest of the row elements of j^{th} column are 0. The efficient multidimensional matrix array computation in the MatLab environment (The MathWorks, Natick, MA) enabled us to create this fast Monte Carlo simulation. This way we can keep track of the internal state of each individual CaM molecule and it allows us to calculate the cycle time and first passage time of Ca^{2+} interactions with CaM.

Estimation of reaction rate constants

All parameter values in the model were taken from experimental data or estimated via parameter optimization (Table 1). The kinetic pathways of Ca^{2+} binding to CaM and subsequent interaction with target protein are shown in Fig. 1 *A*. For the parameter optimization, we used the ordinary differential equation model of the system. For Ng, the experimental data related to Ca^{2+} association to and dissociation from CaM in the presence of Ng, are available (5,6) However, these experiments do not directly measure the individual reaction rate shown in Fig. 1. For example, the Ca^{2+} dissociation from CaM in the presence of Ng contains a convolution of Ca^{2+}/CaM dissociation from Ng and Ca^{2+} dissociation from CaM. We needed to employ parameter optimization strategy to estimate individual kinetic rate from these experimental data. All parameter values are constrained by microscopic reversibility and this thermodynamic principle helped reduce the number of unknown parameters. We employed a brute force stochastic parameter search from a slate of 10^8 different parameter sets followed by nonlinear least-square methods (e.g., Levenberg-Marquardt and trust region method implemented in the MatLab Optimization Toolbox). The final 100 candidate parameter values were tested against experimental data and the best parameter set was chosen (see Table 1 and Fig. 1 *B*). All macroscopic reaction rates were converted to reaction probabilities assuming that the reaction volume is equal to 0.125 μm^3, the size of a small postsynaptic spine in which 1μM of any chemical species equates with 75 molecules. The Ca^{2+} binding kinetics of EGTA used in Fig. 1 *B* were taken from Schuhmeier et al. (14).

Estimation of protein concentrations

The CaM concentration in the dendrite is estimated to be ~20 μM (15). Ng concentration in the hippocampal neurons varies broadly, 70~370 (pmol/mg protein), and is higher in the dendritic spine (8). However, Ng is subject to various posttranslational modifications including PKC-mediated phosphorylation and oxidation, both of which reduce its interaction with CaM (8). The weight and contribution of each of these modifications of Ng are not well known. For this reason, we varied Ng concentrations between 0 and 50 μM in the model and examined its effect.

3D Single-particle trajectory of CaM molecule

The time evolution of the Ca^{2+} binding state of a given CaM molecule was taken from the corresponding simulations in Fig. 4. The Brownian motion of this molecule was created using a Monte Carlo scheme. At each time step ($dt = 1\ \mu s$), we draw two unit-interval uniform random numbers, r_1 and r_2, which define the direction vector ($\sin\theta\cos\varphi$, $\sin\theta\sin\varphi$, $\cos\theta$), where $\theta = \pi r_1$ and $\varphi = 2\pi r_2$, respectively. The mean displacement of a Brownian particle over a time dt is $\sqrt{6Ddt}$, where D (2 $\mu m^2\ s^{-1}$) is the diffusion coefficient of CaM in the cytoplasm (16). A Gaussian distribution (0 mean and $\sqrt{6Ddt}$ variance) was used to determine the jump length (third random number). The shape of the simplified model spine used in our simulations is shown in Fig. 6 *A*. The spine head is modeled as a cube of 500 nm side. A 500-nm-long spine neck is attached to the head. When a CaM molecule collides into the wall (boundary), we impose an elastic collision rule to calculate its trajectory. This way we generate a discretized Brownian trajectory of the CaM molecule under reflective boundary conditions. For this set of simulations, we assume that the diffusion coefficient of CaM molecules is independent of its Ca^{2+} binding state.

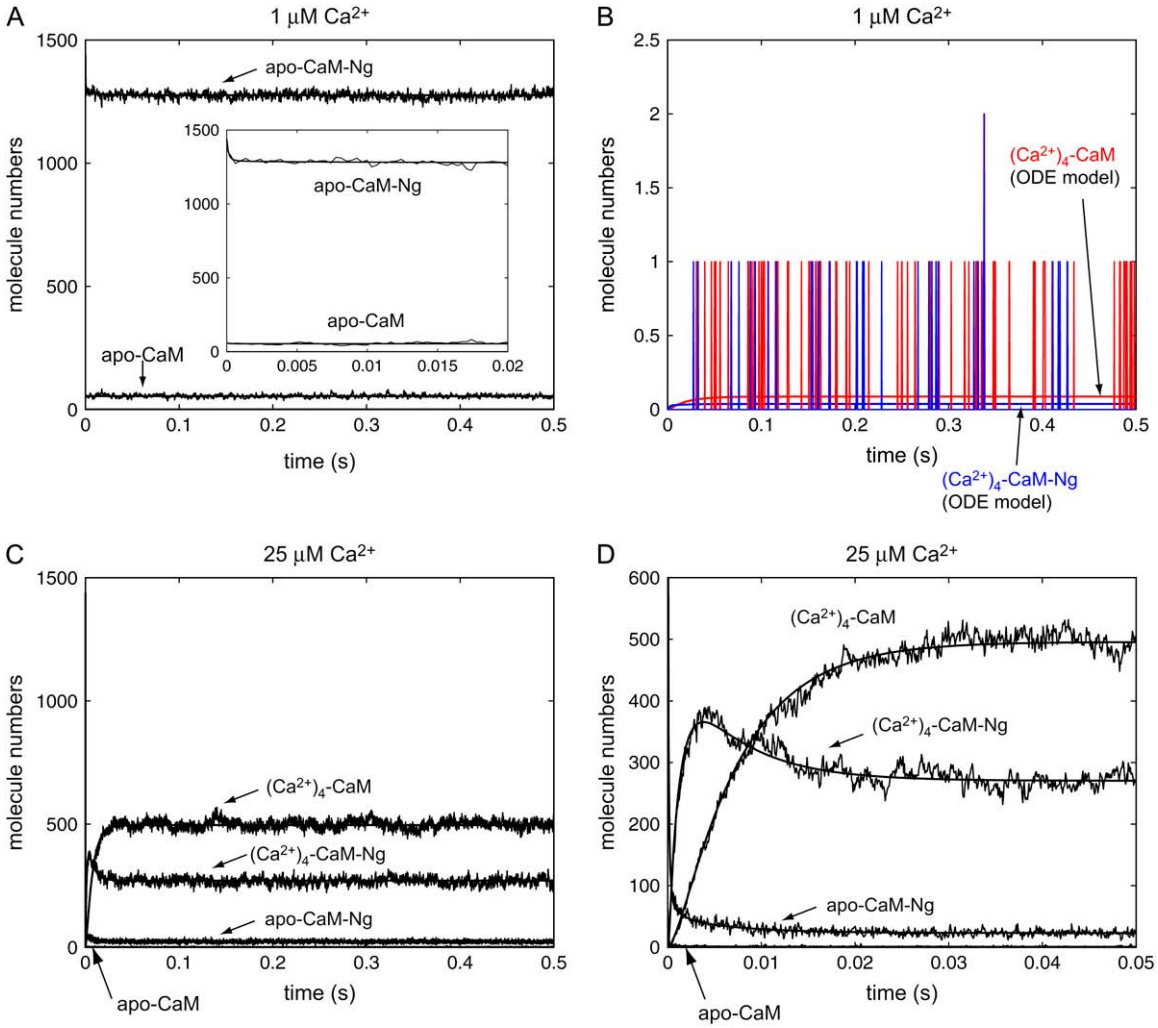

FIGURE 2 Comparing the ODE model and the stochastic model. Extended Gillespie-type model of CaM-Ng interactions (*A–D*, *thin lines*). In these figures, the system (CaM-Ng) was equilibrated with 0 μM of Ca^{2+} for 0.5 s (long enough to reach equilibrium). The Ca^{2+} concentration was then raised to the specified value (1 μM in *A* and *B* and 25 μM in *C* and *D*) at time zero and the time evolutions of the changes in reaction intermediates are shown. The levels of apo-CaM, $(Ca^{2+})_4$-CaM, apo-CaM-Ng complex, and $(Ca^{2+})_4$-CaM-Ng complex reach steady-state levels within 0.5 s. As predicted by a classical view of Ng function, at lower Ca^{2+} concentration, the majority of CaM molecules are in the Ng-bound and Ca^{2+} free state. While at higher Ca^{2+} concentration, a significant amount of CaM becomes fully Ca^{2+} saturated without bound Ng. The thick lines correspond to the same experiments accomplished with ODE simulations. All simulations contain 20 μM (1500 molecules) of CaM and 50 μM (3750 molecules) of Ng. The time evolution of the number of each molecular species is shown (the *vertical axis*). In the ODE models, we calculate the concentration of each reaction intermediate and the concentration is converted to the molecular number by using a formula: 1 μM = 75 molecules. (*A*, *inset*) Early declining phase of the apo-CaM-Ng complex, which takes place during the first 1 ~ 2 ms. (*B*) Time evolution of $(Ca^{2+})_4$-CaM (*red*) and $(Ca^{2+})_4$-CaM-Ng (*blue*) under the same simulation conditions. Only one, or at most two, CaM molecules becomes fully Ca^{2+} saturated at this concentration of Ca^{2+} (1 μM). Thick red and blue lines are results from the corresponding ODE model. (*C* and *D*) Time evolution of the system with 25 μM Ca^{2+}. (*D*) Level of $(Ca^{2+})_4$-CaM-Ng overshoots during the first ~10–20 ms of the simulation before relaxing to the steady-state level.

RESULTS

The mathematical model

CaM is a bi-lobed molecule that has two Ca^{2+}-binding sites within each lobe and Ng interaction with CaM was shown experimentally to increase the rate of Ca^{2+}-dissociation from the sites in the C-terminal lobe (4,5). Fig. 1 *A* shows how this kinetic mechanism is modeled. Each lobe of Ng-free CaM has three different states dependent on the number of bound Ca^{2+} ions: (apo)-CaM, (Ca^{2+})-CaM, and $(Ca^{2+})_2$-CaM (*horizontal arrows* in Fig. 1 *A*). Ng binds each of these three states of the C-lobe of CaM with different affinities (*vertical arrows* in Fig. 1 *A*). Ng changes CaM's affinity toward Ca^{2+} by increasing the dissociation rate (k_{-9}, *thick horizontal arrow* in the C-lobe kinetic pathway, Fig. 1 *A*) but it does not change the Ca^{2+} association rate (5). We assume Ng affects only the C-lobe of CaM as supported by present experimental evidence (6). Thus, the CaM molecule has 18 (6 × 3)

different states. We first constructed an ODE-type model based on experimental data and the parameter values were optimized (see Methods for the details of the parameter optimization). We found a unique region of parameter space in which the optimized dissociation rates of Ca^{2+} and Ng are both consistent with the experimentally observed experimental data on the Ca^{2+}, Ng, and CaM interaction. Fig. 1 *B* shows the goodness of fit of the model (*line*) with experimental data of Ng-induced Ca^{2+} dissociation from CaM (*circles*/*squares*).

Having established the kinetic pathway and the corresponding parameter values, we next calculated the cycle time and passage time of Ca^{2+}/CaM in the presence of varying concentrations of Ng. To date, several mathematical and computational approaches have been developed to calculate reaction times (passage time and cycle time) and their statistical distribution at the single molecule level (17–21). Analytic approaches (17,21) are often more valuable than numerical solutions because of the insights that analytic methods provide into the dependence of these reaction times on underlying kinetic parameters. However, deriving analytic formulas for the system of 18 different activation states (Fig. 1 *A*) is an arduous task. Furthermore, the resulting formula may not be simple enough to understand the role and contribution of each kinetic parameter in the reaction scheme. For this reason, we developed a Monte Carlo scheme using an extended version of the Gillespie-type stochastic simulation (11) that enables us to keep track of the activation state of each CaM molecule in the system. The details and underlying principle of this numerical algorithm are described in the Methods. In brief, we treat each individual CaM molecule as if they were different chemical species but that have the potential to undergo the exact same chemical reactions with Ng and Ca^{2+}. With this numerical scheme, we can generate the stochastic reaction trajectory of individual CaM molecules during the simulation. This way, the calculations of the first passage time and the cycle time become straightforward. Our numerical method is as exact and accurate as the conventional Gillespie-type algorithm.

Fig. 2 *A* ~ 2 *D* show the time evolutions of this stochastic simulation compared against the original ODE model of the Ca^{2+}-Ng-CaM system. The simulations contain 1500 molecules of CaM (equivalent to 20 μM of CaM in a small volume of average postsynaptic spine; ~0.125 μm^3) (22) and 3750 molecules of Ng (i.e., 50 μM) interacting with constant levels of Ca^{2+} (raised from 0 μM at time zero: low Ca^{2+} level, 1 μM in Fig. 2, *A* and *B* and high Ca^{2+} level, 25 μM in Fig. 2, *C* and *D*). Trajectories of the numbers of apo-CaM, $(Ca^{2+})_4$-CaM (i.e., fully Ca^{2+} saturated CaM), apo-CaM-Ng, and $(Ca^{2+})_4$-CaM-Ng are taken from a single simulation run (*thin lines*) and compared against the ODE model (*thick solid lines*). As shown, the stochastic simulation follows the same time evolution as the ODE model (Fig. 2 *A*, *inset*, *C* and *D*). The average of our stochastic simulation converges at the ODE result. At lower Ca^{2+} concentration (1 μM, Fig. 2 *A*), most CaM molecules are bound to Ng and are in the Ca^{2+} free apo-state. Only one or at most a few CaM molecules can reach the fully Ca^{2+} saturated state in the entire spine volume (see the *red* [$(Ca^{2+})_4$-CaM] and *blue* [$(Ca^{2+})_4$-CaM-Ng] *vertical spikes* in Fig. 2 *B*, which are taken from the stochastic simulation). At higher (25 μM) Ca^{2+} concentration (Fig. 2 *C*), the amounts of Ca^{2+} saturated CaM (free of Ng) are dramatically increased. These results are consistent with the previously proposed role of Ng as a CaM reservoir, releasing CaM upon Ca^{2+} stimulation (9). Fig. 2 *D* is a shorter timescale version of Fig. 2 *C* and it shows that the concentrations of two molecular species, apo-CaM-Ng and $(Ca^{2+})_4$-CaM-Ng, overshoot before they relax to the steady-state level.

Cycle time

Fig. 3 *A* is a reaction trajectory of a single CaM molecule, taken from the stochastic simulation containing 25 μM (fixed) of Ca^{2+}, 20 μM CaM, and 50 μM of Ng (Fig. 2 *C*). Here we plot the number of bound Ca^{2+} ions to this single CaM molecule at each time point resulting in this stairstep graph. At 25 μM Ca^{2+}, the CaM molecule spends most of the time flip-flopping between the two Ca^{2+} ion-bound state, three Ca^{2+} ion-bound state, and the fully Ca^{2+}-saturated state. We define cycle time as the time interval between two consecutive Ca^{2+} saturated states (two examples are indicated by *double-headed arrows*). The CaM molecule has the potential to sequentially visit each activation state with different probability and goes through many different combinations of activation states before returning to the fully Ca^{2+} saturated state. In contrast, at lower Ca^{2+} (1 μM, fixed) concentration, the CaM molecule is in a partially Ca^{2+} saturated state or apo-state for most of the time (Fig. 3 *B*). Note that the time axis in Fig. 3 *B* is significantly longer than in Fig. 3 *A*.

Interestingly, once achieved, the lifetime of the Ca^{2+} saturated state at either 25 μM (Fig. 3 *A*) or 1 μM (Fig. 3 *B*) Ca^{2+} is similar (~450–500 μs in both simulations). The mean lifetime of $(Ca^{2+})_4$-CaM (with or without bound Ng) is the inverse of the sum of rates of reaction pathways leaving from this molecular species, i.e., the dissociation rates of Ca^{2+} from this complex (N-lobe and C-lobe). The lifetime of Ca^{2+}-saturated CaM is largely determined by the faster Ca^{2+} dissociation rate from the N-lobe (2000 s^{-1}, Fig. 1 and Table 1). Because Ng only influences the Ca^{2+} dissociation rate from the C-terminal lobe of CaM, its presence has only a negligible effect on the lifetime of the Ca^{2+}-saturated CaM.

The stochastic fluctuations of the cycle time is analyzed in Fig. 3 *C*, which shows the histogram of cycle time distributions calculated from 1000 simulation runs at 25 μM Ca^{2+} (similar to Fig. 3 *A*). In addition, the cycle time depends on the Ca^{2+} concentration. Fig. 3 *D* is the histogram of cycle time for 1 μM Ca^{2+}, which shows a larger variation in the distribution than with the higher Ca^{2+} concentration (note that the *time axis* in Fig. 3 *D* is 1000-fold longer than in Fig. 3 *C*).

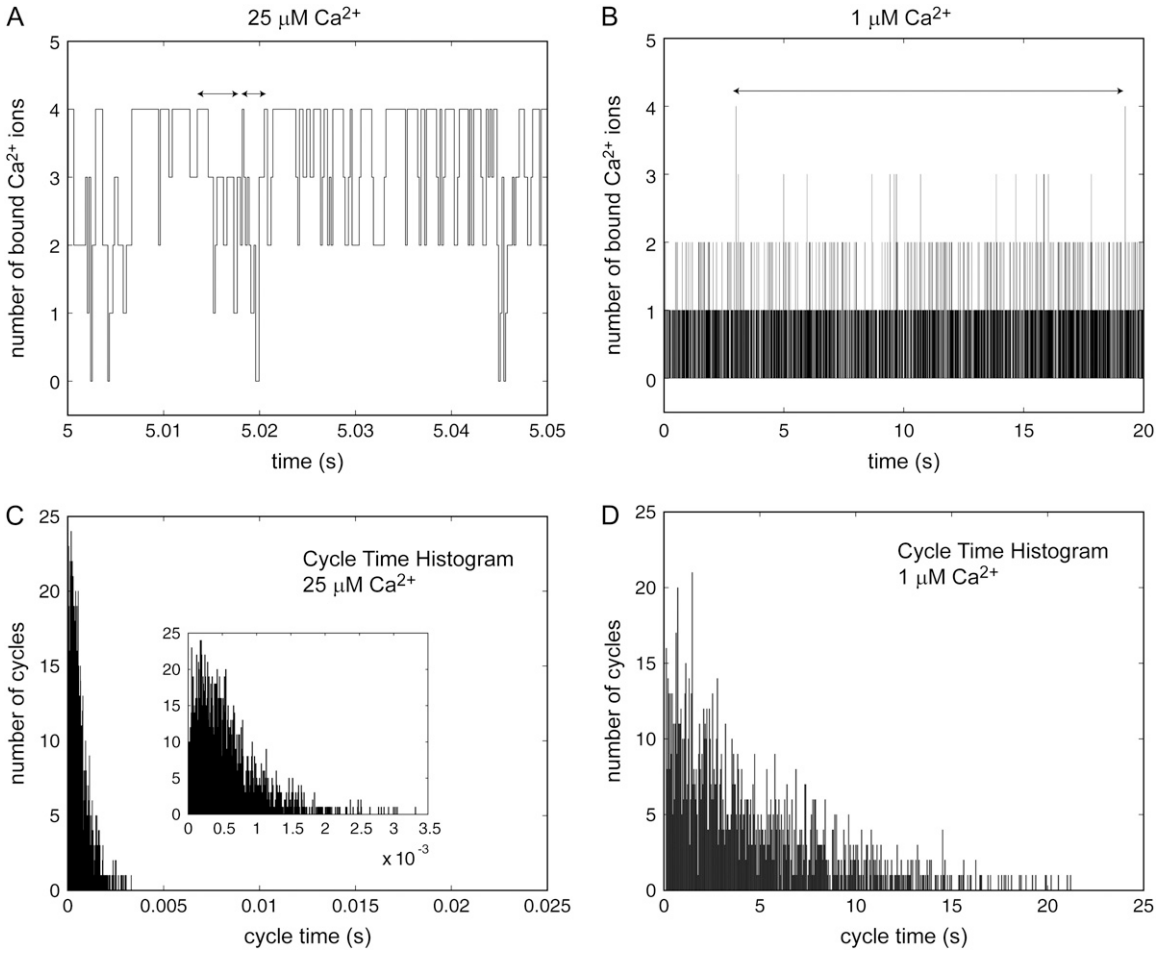

FIGURE 3 Reaction trajectories of single CaM molecules and histograms of their mean cycle time. (*A*) Each CaM molecule has the potential to undergo a cycle of Ca^{2+} binding/dissociation and Ng binding/dissociation. A single simulation run of a randomly selected CaM molecule is shown. The stairstep graph shown here indicates the number of Ca^{2+} ions bound to this CaM molecule at each time point. The time interval between two consecutive Ca^{2+} saturated states is the cycle time and it undergoes stochastic fluctuation (two examples are indicated by *double-headed arrows*). This simulation contains 25 μM Ca^{2+}, 20 μM (1500 molecules) of CaM and 50 μM (3750 molecules) of Ng. (*B*) Similar analysis performed at a lower Ca^{2+} concentration (1 μM). As above, we show a single simulation run of one CaM molecule. The stairstep graph shows the number of bound Ca^{2+} ions to this particular CaM molecule. The cycle time indicated by a double-headed arrow is much longer than that when 25 μM of Ca^{2+} is present in the simulation. Note the time axis is expanded relative to that shown in panel *A*. (*C* and *D*) Histogram of cycle time distributions taken from 1000 simulation runs at different Ca^{2+} concentrations (25 μM in *C* and 1 μM in *D*).

In Fig. 4, we plot the mean cycle time as a function of Ca^{2+} levels (0.3 $\sim$ 100 μM) with different concentrations of Ng: 0 μM (*solid dots* and *line*), 30 μM (*solid crosses* and *line*), and 50 μM (*solid circles* and *line*). The range of Ca^{2+} concentrations used here spans the levels of Ca^{2+} transients measured in the dendritic spine (23). Without Ng, the mean cycle time (the time between visits to the fully Ca^{2+} saturated state) increases as the Ca^{2+} concentration is lowered (Fig. 4, *solid circles* and *line*). The curve of the Ca^{2+}-dependent mean cycle time becomes steeper as Ng concentration is increased. At higher Ng concentrations, a given CaM molecule has a higher probability of undergoing Ng binding and Ca^{2+} dissociation via $(Ca^{2+})_2$-CaM (C-lobe)-Ng (*thick horizontal arrow* in Fig. 1 *A*). Once Ca^{2+} dissociates, the CaM molecule spends a long time alternating between the apo- state and the single Ca^{2+}-bound state (Fig. 1 *A*) before the second Ca^{2+} binds. In fact, the Ca^{2+} dissociation rate from (Ca^{2+})-CaM (C-lobe) is extremely fast, $>5200\ s^{-1}$, and is higher than the speed of the second Ca^{2+} association (Fig. 1 *A*).

Dissection of Ng action

If the rapid Ca^{2+} dissociation pathways from $(Ca^{2+})_2$-CaM (C-lobe)-Ng or from (Ca^{2+})-CaM (C-lobe)-Ng is the major mechanism that controls the mean cycle time, modifications of these rates (k_{-8} and k_{-9}, *two leftward horizontal arrows* in the *upper half* of the *C-lobe CaM diagram* in Fig. 1 *A*) should influence the mean cycle time. We tested this hypothesis by creating a series of simulated Ng mutants that have different dissociation rates in these steps of the kinetic scheme. In the first mutant, which we call the inactive

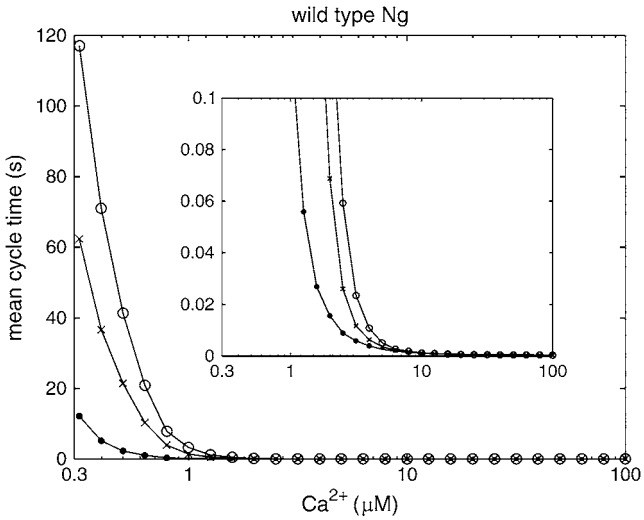

FIGURE 4 The effect of Ca^{2+} and Ng concentration on the mean cycle time of Ca^{2+}/CaM. The mean cycle times are calculated (over 1000 simulation runs) and plotted with various Ca^{2+} concentrations (*horizontal axis*) in the presence of 0 μM (*solid dots* and *line*), 30 μM (i.e., 2250 molecules, *solid crosses* and *line*), and 50 μM (i.e., 3750 molecules, *solid circles* and *line*) Ng. All simulations contain 20 μM (1500 molecules) of CaM. The mean cycle time becomes shorter than 100 ms for Ca^{2+} concentrations $>\sim 1$ μM. Note the *y* axis (the mean cycle time) of the inset is $\sim$1000-fold smaller than the main figure.

mutant, we modified the rate k_{-9} in Fig. 1 *A*. This mutant Ng does not change the Ca^{2+} dissociation rate from CaM (*rectangle* in Fig. 5 *A*, *inset*) like wild-type Ng does. It binds apo-CaM (C-lobe) and Ca^{2+}-saturated CaM (C-lobe) with the same affinity as a consequence of the thermodynamic principle of microscopic reversibility (Fig. 5 *A*, *inset*, and for the specific parameters, see Table 2). Since this inactive Ng mutant does not accelerate the Ca^{2+} dissociation from CaM, we hypothesized that there would be no change in the mean cycle time. As predicted, the mean cycle times with 30 μM (*solid crosses* and *line*) and 50 μM (*solid circles* and *line*) of Ng are over those of 0 μM (*solid dots* and *line*) Ng (Fig. 5 *A*). These effects on the mean cycle time are mainly due to the reduction of the Ca^{2+} dissociation we made in the mutant and are largely independent of the choice of Ng association and dissociation rates. In fact, if microscopic reversibility was ignored and only the Ca^{2+} dissociation rate (k_{-9}) were altered in the simulations, we obtained a similar mean cycle time as in the inactive mutant (data not shown). These results show that the mean cycle time is dominated by the Ca^{2+} binding kinetics of the CaM (C-lobe)-Ng complex.

What will happen to the mean cycle time if we cause Ng to decrease the other Ca^{2+} dissociation step from the C-terminal lobe of CaM (k_{-8} in Fig. 1 *A*)? The simulation result in Fig. 3 *B* indicated that in the presence of Ng, the CaM molecules (C-lobe) reside for long periods in the apo- or one Ca^{2+}-ion bound state, due to the large Ca^{2+} dissociation rate ($k_{-8} > 5200\ s^{-1}$). So, if we reduce this dissociation rate (k_{-8}) in the simulations, then we may be able to change the mean cycle time even when Ng still accelerates Ca^{2+} dissociation from the fully Ca^{2+}-saturated CaM. In this mutant, which we call biphasic Ng, we decreased (30-fold) the Ca^{2+} dissociation rate (k_{-8}) from (Ca^{2+})-CaM (C-lobe)-Ng while maintaining the 30-fold accelerated Ca^{2+} dissociation (k_{-9}) from the fully saturated C-lobe (see the *inset* of Fig. 5 *B* and for the specific parameters see Table 2). The calculated mean cycle time in this mutant is shorter than wild-type Ng, supporting our hypothesis that the intermediate molecule, (Ca^{2+})-CaM (C-lobe)-(mutant) Ng, has a higher probability of returning to the fully Ca^{2+} saturated state than with wild-type Ng (compare Fig. 4 and Fig. 5 *B*). As in Fig. 5 *A*, the observed reduction in the mean cycle time is mainly due to the reduced Ca^{2+} dissociation at the step k_{-8} and is independent of the choice of Ng association and dissociation rates (data not shown).

What will happen to the mean cycle time if we increase the Ca^{2+} association rate that leads to the Ca^{2+}-saturated C-lobe (*thick rightward horizontal arrow* in the reaction scheme in Fig. 5 *C*)? We test this by creating another mutant, which we call the PEP-19-like mutant. This mutant binds the Ca^{2+} bound form of CaM (C-lobe) with the same affinity as apo-CaM. This simulated mutant Ng increases both Ca^{2+} association and dissociation rates of CaM 30-fold higher than that of intact CaM upon binding (*rectangle* in Fig. 5 *C reaction scheme* and Table 2). Therefore, the overall Ca^{2+} affinity is the same as intact CaM, but the association and dissociation rates are both increased (Fig. 5 *C reaction scheme*). A small neuronal IQ motif protein, PEP-19, has these biochemical effects on the Ca^{2+}-binding kinetics of CaM (7). With this PEP-19-like mutant, the mean cycle time is approximately the same as the inactive Ng or no Ng control (Fig. 5 *C*). The compensatory effect of the increased association rate and the increased dissociation rate of Ca^{2+} of the pathway dictates the dynamics of this PEP-19-like mutant. Again, the binding kinetics of Ng to the apo- and partially Ca^{2+}-saturated CaM has negligible effects on the mean cycle time as above (data not shown).

3D trajectory combined with the mean cycle time of a single CaM molecule

How does the mean cycle time influence the spatial pattern of CaM activation? To illustrate this, we generated a trajectory for a CaM molecule following simple Brownian motion, alternating between the fully Ca^{2+}-saturated state (drawn in *red*) and partially Ca^{2+}-saturated state (drawn in *blue*). Brownian motion of this molecule was created using a Monte Carlo scheme described in the Methods. The diffusion coefficient of CaM used here is 2 $\mu m^2\ s^{-1}$ (16) and we use a simple geometric model of a postsynaptic spine for illustration. The time evolution of the Ca^{2+} binding state of this molecule was taken from our simulations in Fig. 4. The total simulation time is 200 ms. Comparing the 3D trajectory of a CaM molecule at 2.5 μM Ca^{2+} concentration

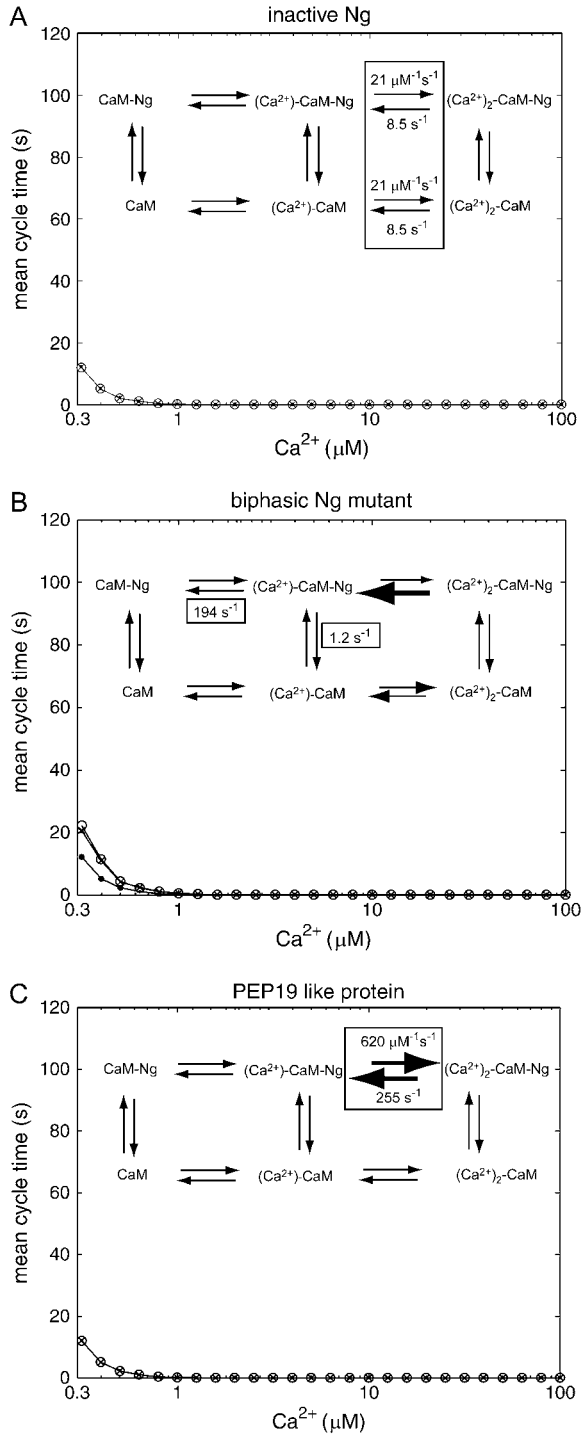

FIGURE 5 The mean-cycle time calculated for different artificial mutants of Ng. All simulations contained 20 μM (1500 molecules) of CaM and 0 μM of Ng (control, *solid dots* and *line*) or 30 μM (i.e., 2250 molecules) of (mutant) Ng (*solid crosses*, *circles*, and *line*) or 50 μM (i.e., 3750 molecules) of (mutant) Ng (*solid circles* and *line*). The mean cycle time is calculated and plotted for each Ca^{2+} concentration. All parameter values for the different Ng mutants used in these simulations are summarized in Table 2. The inset of the figure highlights the major parameter values changed in each mutant. (*A*) Inactive Ng. A simulated mutant Ng (inactive Ng, *solid circles* and *line*) that binds CaM with the same affinity as wild-type Ng but it does not change the Ca^{2+} binding kinetics of CaM (*rectangle* of rates in the *inset*). The microscopic reversibility principle demands the corresponding binding kinetics of Ng to CaM (*vertical arrows*) need to be adjusted. We assume Ng binds to and dissociates from Ca^{2+}-bound CaM at the same rate as apo-CaM (k_5 and k_{-5} in Fig. 1 *A*). As explained in the text, the values of these Ng binding kinetic rates do not influence the mean cycle time. (*B*) Simulations with a biphasic Ng mutant. Another mutant Ng, in which the dissociation rate of Ca^{2+} from the (Ca^{2+})-CaM-Ng complex is reduced 30-fold (rates affected are identified within *rectangles*). The dissociation of Ca^{2+} from the fully saturated C-lobe (i.e., $(Ca^{2+})^2$-CaM-Ng) is the same as wild-type Ng. (*C*) Simulations with a third mutant Ng, which we call PEP-19-like protein. In this mutant, both Ca^{2+} association and dissociation rates to the C-terminal lobe are 30-fold faster than faster than wild CaM (rates affected are identified within the *rectangle*). It implies this mutant Ng binds apo- and Ca^{2+} bound CaM with the same affinity (due to microscopic reversibility).

TABLE 2 Parameters used in the mutant Ng models

Symbol*	Fig. 5 *A*	Fig. 5 *B*	Fig. 5 *C*	Units
k_1	426	426	426	$\mu M^{-1}\ s^{-1}$
k_2	21	21	21	$\mu M^{-1}\ s^{-1}$
k_8	426	426	426	$\mu M^{-1}\ s^{-1}$
k_9	21	21	21	$\mu M^{-1}\ s^{-1}$
k_{-1}	5115	5115	5115	s^{-1}
k_{-2}	8.5	8.5	8.5	s^{-1}
k_{-8}	5115	5115	5115	s^{-1}
k_{-9}	8.5	255	255	s^{-1}
k_5	28	28	28	$\mu M^{-1}\ s^{-1}$
k_6	28	28	28	$\mu M^{-1}\ s^{-1}$
k_7	28	28	28	$\mu M^{-1}\ s^{-1}$
k_{-5}	36	36	36	s^{-1}
k_{-6}	36	1.2	36	s^{-1}
k_{-7}	36	36	36	s^{-1}

The mutant Ng values are identified by the figure numbers. The insets of Fig. 5 show only the major parameter values changed in the mutant that influence the dynamics of the system.

*The symbols for each kinetic rate are indicated in Fig. 1 *A*. Only the C-terminal lobe parameter values are changed in the mutants.

in the presence (50 μM, Fig. 6 *A*) or absence of Ng (Fig. 6 *B*) demonstrates that Ng limits the effective range of action of Ca^{2+}-saturated CaM. As stated earlier (Fig. 4), Ng increases the time that a given CaM molecule spends in a partially Ca^{2+} saturated or apo-state. The lifetime of the fully Ca^{2+} saturated state, however, is the same (~450–500 μs) and is independent of Ng. As a result, Ng decreases the frequency of CaM alternating between the red (Ca^{2+} saturated, active) state and blue (partially saturated, inactive) state in a given time period. In other words, more red spots in Fig. 6 *B* than in Fig. 6 *A*. For perspective, the average distance a CaM molecule travels while in the Ca^{2+}-saturated state (*red spots*) is ~75 nm, which is ~3–4 times' larger than the size of a single CaM-dependent protein kinase II (CaMKII) holoenzyme (~20 nm) in the postsynaptic spine.

As we increase the Ca^{2+} concentration, the duration of the blue state becomes shorter. At 25 μM Ca^{2+}, even in the presence of 50 μM Ng, the blue state is $<\sim$75 μs, a time duration that a CaM molecule can travel over a distance only slightly larger than the size of CaMKII. Accordingly, a given

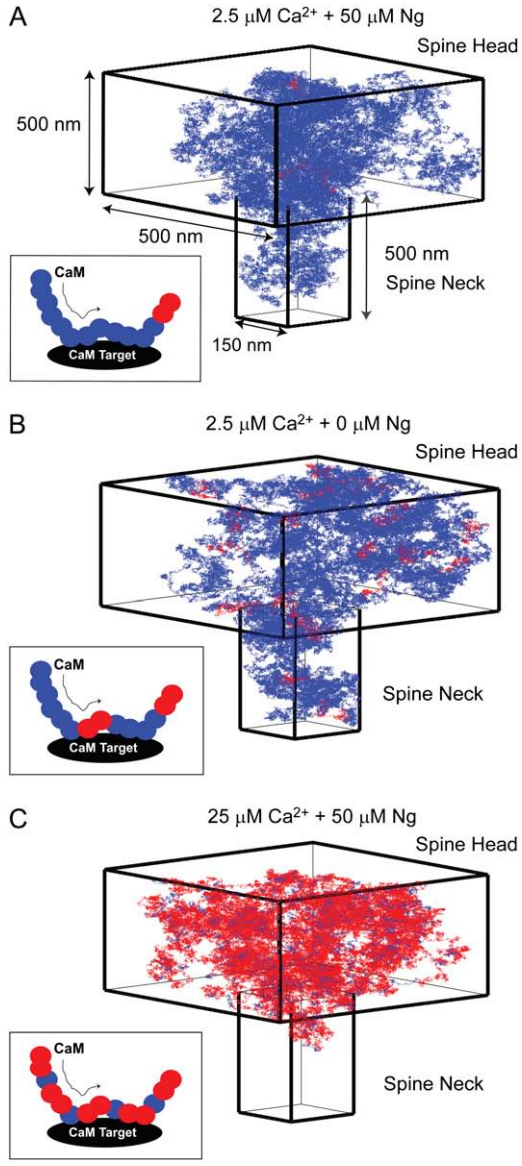

FIGURE 6 Single particle trajectory of a CaM molecule alternating between Ca^{2+} saturated and partially Ca^{2+} saturated states, bounded within a model synaptic spine. The time evolution of a single molecule CaM taken from the simulation (Fig. 4 and see Methods) was used to generate a 3D trajectory of its Brownian motion (over 200 ms) in the postsynaptic spine. The intracellular diffusion coefficient of CaM was 2 $\mu m^2 s^{-1}$. The trajectory is plotted red when it is in the Ca^{2+} saturated state and in blue otherwise. The time step for calculating the 3D Brownian trajectory in this simulation was 1 μs. The concentrations of Ca^{2+} are 2.5 μM (*A*), 2.5 μM (*B*), and 25 μM (*C*), respectively. Each simulation contains 50 μM (*A*), 0 μM (*B*), and 50 μM (*C*) of Ng. Panels *A* and *B* compare the effect of Ng on the mean cycle time. The influence of higher Ca^{2+} concentration is illustrated between panels *A* and *C*. The inset of each panel is a cartoon illustration of a *single* CaM molecule (*solid circle* in *red* or *blue*) searching for its target (CaM-target, *solid ellipsoid*) via a random walk. The CaM molecule changes its Ca^{2+} bound state while it moves in the space: blue (apo- or partially Ca^{2+} saturated state) and red (fully Ca^{2+} saturated state). The lifetime of red state is the same for all simulation conditions (*A–C*; see text for more details). The duration of the blue state controls the frequency that a given CaM molecule flip-flops between red and blue states. Note the ratios of blue state and red state in the insets are not necessarily proportional to the corresponding figure.

CaM molecule flip-flops between the blue and red states many times (~350 times) during a give time period (200 ms) and at 25 μM Ca^{2+} explores a high proportion of the 3D volume in the fully Ca^{2+}-saturated (*red*) state (Fig. 6 *C*). Note in Fig. 6 *C* that a large number of red spots in the figure mask the short strings of blue spots.

The inset of each panel of Fig. 6 is a cartoon illustration of a single CaM molecule (*solid circle* in *red* or *blue*) searching for its target (CaM-target, *solid ellipsoid*) via a random walk. The CaM molecule changes its Ca^{2+} bound state between blue and red while it moves in the space (indicated by a *solid arrow*). If the mean cycle time is long (Fig. 6 *A*), the CaM molecule spends most of its time in the blue state. The probability that the CaM molecule collides into its target while in the red state is extremely low. This probability increases, as the mean cycle time becomes shorter (Fig. 6, *B* and *C*). Since the random walk is the only way that a CaM molecule can find its target, the mean cycle time is an effective way of controlling CaM's spatial range of action during the Ca^{2+} transient. Ng, in addition to its role as a CaM reservoir, has the capacity to regulate the spatial pattern of CaM action.

First passage time

So far, we have studied the behavior of the Ng-CaM system under constant levels of Ca^{2+}. The response of this system to the time-varying Ca^{2+} signal may differ significantly from its steady-state dynamics. The stochastic algorithm presented here is fully capable of analyzing such a behavior as long as we assume Ca^{2+} is well stirred and homogeneous. Here we present a simple quantity to asses the temporal dynamics of the Ng-CaM. We calculate the (mean) first passage time, the length of transition time required for a CaM molecule to reach the fully Ca^{2+} saturated state from a basal (apo-) state in the presence or absence of Ng. If, for example, the first passage time were longer than the duration of the Ca^{2+} transient, there would be no CaM activation of the postsynaptic signaling system. CaM molecules will not enter the high frequency flip-flopping mode of behavior as shown in Fig. 6 *C*.

To calculate the first passage time, we increase the Ca^{2+} concentration in a steplike function, from 0 μM to a given value and keep it constant while calculating the passage time for each CaM molecule in the simulation. Fig. 2 *A* (*inset*), *B*, and *D*, has already shown such a transient behavior for a population of CaM molecules, here we employ a single molecule level approach to analyze the transient dynamics. Fig. 7 is the result of such a calculation. The simulation contains 20 μM (1500 molecules) of CaM and 0 (*solid dots* and *line*) or 50 (*solid circles* and *line*) μM of wild-type Ng and the mean first passage time is plotted as a function of the final level of Ca^{2+}. Not surprisingly, Ng slows down the transition from the apo- to the fully Ca^{2+} saturated state. In contrast, the same amount (50 μM) of PEP-19-like protein

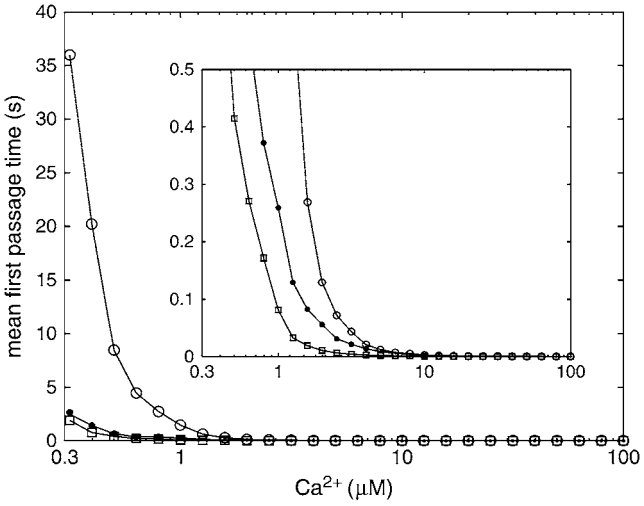

FIGURE 7 First passage time of Ca^{2+} binding to CaM. The mean transition time of CaM going from the basal (apo-) state to reach the fully Ca^{2+} saturated was calculated and plotted as a function of Ca^{2+} concentration. The simulation conditions are the same as in Figs. 4 and 5. The solid dots and line indicate a control simulation without Ng. The effect of wild-type Ng (*solid circles* and *line*) and a PEP-19-like protein (*solid square* and *line*) are compared against the control. The concentrations of Ng and PEP-19-like proteins are 50 μM (3750 molecules).

(*solid squares* and *line*) reduces (~20–80%) the first passage time relative to the control (0 μM Ng). As with the mean cycle time, the effect of either Ng or PEP-19 on the transition into the fully Ca^{2+}-saturated state of CaM become negligible as the Ca^{2+} levels rise (>10 μM) (Fig. 7, *inset*).

DISCUSSION

Ng has been hypothesized as a CaM storage protein that releases CaM upon Ca^{2+} stimulation and recent modeling work on Ng explored its role primarily based on this assumption (24). In this work, we have investigated other possible functionality of Ng by evaluating the experimentally documented increase Ng has on accelerating Ca^{2+} dissociation from the C-terminal lobe of CaM (5,6). Our work suggests that, although the interaction of Ng with Ca^{2+} bound CaM is transient, Ng has a significant impact on the mean cycle time of Ca^{2+}/CaM via accelerated Ca^{2+} dissociation from the C-terminal lobe of CaM. Changing this dissociation rate or accelerating the Ca^{2+} association rate of the same pathway diminished the effect of Ng (Fig. 5). Interestingly, another neuronal IQ-motif protein enriched in cerebellar Purkinje cells, PEP-19, increases the dissociation rate as well as the association rate of Ca^{2+} to the same degree (7). We found that the mean cycle time of Ca^{2+}/CaM with the PEP-19-like protein is close to that of CaM alone for all Ca^{2+} concentrations tested (0.3–100 μM) (Fig. 5 *C*). These results suggest that Ng and PEP-19 have very different effects on the spatiotemporal pattern of CaM action and that the physiological role of PEP-19 in cerebellar Purkinje cells (and other cells that contain PEP-19) may be different from those of Ng in hippocampal CA1 neurons. It would be interesting to see how GAP43 (neuromodulin) (3), another neuronal IQ motif protein enriched in the presynaptic terminal, regulates the Ca^{2+} binding kinetics of CaM. Our modeling scheme will provide a convenient tool to evaluate the spatiotemporal impact GAP43 may have on the presynaptic Ca^{2+} signaling cascade.

In fact, Ng sets a sharp transition of the mean cycle time between two concentration zones of Ca^{2+}: lower zone of <1 μM and higher Ca^{2+} of 10~20 μM or more. As illustrated in Fig. 6, at high Ca^{2+} concentrations (>10 μM) with or without Ng present, the CaM molecules remain in the fully Ca^{2+} bound active state and can extensively search for targets via a blind random walk. In the presence of Ng and at lower Ca^{2+} concentrations (e.g., ~2.5 μM or below), the frequency of entering the fully Ca^{2+}-saturated state is dramatically reduced and CaM molecule remains in an inactive (partially Ca^{2+} saturated or unbound state) for long periods. During 200 ms of the simulation time in Fig. 6, CaM molecules (with diffusion coefficients of 2 $\mu m^2\ s^{-1}$) explore most of the volume of the postsynaptic spine. Therefore, Ng has a significant impact on the spatiotemporal pattern of postsynaptic CaM signaling system via its effects on the mean cycle time of CaM.

In addition, our analyses on the first passage time indicates that Ng also controls the transition time required for a CaM molecule to reach its Ca^{2+}-saturated state. Again, Ng sets a relatively sharp transition of the first passage time between low and high Ca^{2+} concentrations. The combined biological effects of Ng on the first passage time and the mean cycle time would become clearer when one considers the Ca^{2+}/CaM-binding properties of PP2B (or calcineurin) and Ca^{2+}/CaM-dependent protein kinase II (CaMKII), two major downstream targets of CaM that play an important role in the induction of synaptic plasticity. PP2B activation is fast and it decays slowly because of its high affinity toward Ca^{2+}-saturated CaM (25). Therefore, a small number of Ca^{2+}-activated CaM transitions would be sufficient to activate PP2B. In contrast, CaMKII requires two Ca^{2+}-activated CaM molecules to bind to it simultaneously to initiate the process of autophosphorylation (26). Thus, the probability that two Ca^{2+}-saturated CaM molecules will collide into the same CaMKII molecule sharply depends on the mean cycle time. The longer the mean cycle time, the smaller the probability of this simultaneous collision occurring, blunting the autophosphorylation of CaMKII.

Note that the ODE type analysis utilized to generate the results in Fig. 2 must be clearly distinguished from the single molecule-level analyses (the cycle time and first passage time) presented in Figs. 3–7. The former analysis describes the average number of CaM molecules in each activation state while the latter analyses characterize the dynamics of single CaM molecules. In fact, the cycle time and first passage time are not straightforward functions of the average

number of molecules in each state. The regulation of the stochastic dynamics (fluctuation) of CaM by Ng at the single molecule-level must be differentiated from its macroscopic role (e.g., CaM reservoir). Nonetheless, these two aspects of Ng function act in synergy to set a sharp transition between low and high Ca^{2+} concentrations. Lowering Ca^{2+} concentration and increasing Ng concentration result in fewer (fully) Ca^{2+}-saturated CaM molecules and a longer time period that each CaM molecule spends in partially Ca^{2+}-saturated states.

We can draw three general conclusions from these results. Ng would decrease the probability of all enzymes being activated at low intracellular Ca^{2+} concentration by minimizing the probability of CaM entering the fully Ca^{2+}-saturated state. At intermediate ($\sim$1.0–10 μM) Ca^{2+} concentrations, Ng continues to have an impact, but depending on the properties of the different Ca^{2+}/CaM target enzymes, some (like PP2B) will become preferentially activated over others (like CaMKII). Finally, when Ca^{2+} concentrations rise beyond $\sim$10 μM, Ng effects disappear and a given CaM molecule flip-flops between partially Ca^{2+}-saturated and fully Ca^{2+}-saturated state many times during a give time period and it explores a high proportion of the 3D volume in the fully Ca^{2+}-saturated state. It is also important to note that the interaction of Ng with CaM is affected by both phosphorylation (via the protein kinase C pathway) and oxidation (6,8–10), which provide additional pathways for controlling Ng's capacity to influence the CaM signaling system. Thus, Ng serves as a tunable gate that produces significant effects on the activation of major postsynaptic signaling molecules underlying the synaptic function.

The stochastic simulation algorithm presented here relies on an assumption: the chemical species are well stirred and homogeneous. As soon as one considers the time-varying Ca^{2+} transients in the spine, this assumption becomes invalid. One needs to take into account the presence of micro- or nanodomains of Ca^{2+} near channel pores as well as the diffusion of Ca^{2+}-binding proteins (27). In addition, the cellular interior is a complex milieu and the cytoplasm is full of mobile and immobile obstacles. This demands the development of a stochastic simulator that can handle molecule-by-molecule chemical reactions while they interact and move in the complex and nonhomogeneous environment (28–30). We are presently developing such a simulator (30). In addition, because of Ng's impact on regulating Ca^{2+}-binding to CaM, Ng will also influence Ca^{2+} dynamics (31). The accelerated Ca^{2+} dissociation from CaM molecule by Ng will increase the concentration of free Ca^{2+} and this effect may also play a role in shaping the Ca^{2+} transient during synaptic stimulation. These issues also need to be addressed in future modeling studies.

We thank Dr. Naveed Aslam for helpful discussions.

This work was supported by U.S. National Institutes of Health grant No. GM069611 and grant No. NS038310. Y.K. also gratefully acknowledges support from the Institutional Training Grant on Neuroplasticity (No. NS 041226) during the early phase of this work.

REFERENCES

1. Yang, S. N., Y. G. Tang, and R. S. Zucker. 1999. Selective induction of LTP and LTD by postsynaptic $[Ca]_i$ elevation. *J. Neurophysiol.* 81: 781–787.
2. Malenka, R. C., J. A. Kauer, D. J. Perkel, M. D. Mauk, P. T. Kelly, R. A. Nicoll, and M. N. Waxham. 1989. An essential role for postsynaptic calmodulin and protein kinase activity in long-term potentiation. *Nature.* 340:554–557.
3. Xia, Z., and D. R. Storm. 2005. The role of calmodulin as a signal integrator for synaptic plasticity. *Nat. Rev. Neurosci.* 6:267–276.
4. Babu, Y. S., J. S. Dack, T. J. Greenhough, C. E. Bugg, A. R. Means, and W. J. Cook. 1985. Three-dimensional structure of calmodulin. *Nature.* 315:37–40.
5. Gaertner, T. R., J. A. Putkey, and M. N. Waxham. 2004. RC3/Neurogranin and Ca^{2+}/calmodulin-dependent protein kinase II produce opposing effects on the affinity of calmodulin for calcium. *J. Biol. Chem.* 279:39374–39382.
6. Gaertner, T. 2004. A novel mechanism for regulation of calmodulin signaling by RC3. PhD thesis. University of Texas Houston Medical School, Houston, TX.
7. Putkey, J. A., Q. Kleerekoper, T. R. Gaertner, and M. N. Waxham. 2003. A new role for IQ motif protein in regulating calmodulin function. *J. Biol. Chem.* 278:49667–49670.
8. Huang, K.-P., F. L. Huang, T. Jager, J. Li, K. G. Reymann, and D. Balschun. 2004. Neurogranin/RC3 enhances long-term potentiation and learning by promoting calcium-mediated signaling. *J. Neurosci.* 24:10660–10669.
9. Gerendasy, D. D., S. R. Herron, J. B. Watson, and J. G. Sutcliffe. 1994. Mutational and biophysical studies suggest RC3/neurogranin regulates calmodulin availability. *J. Biol. Chem.* 269:22420–22426.
10. Krucker, T., G. R. Siggins, R. K. McNamara, K. A. Lindsley, A. Dao, D. W. Allison, L. de Lecea, T. W. Lovenberg, J. G. Sutcliffe, and D. D. Gerendasy. 2002. Targeted disruption of RC3 reveals a calmodulin-based mechanism for regulating metaplasticity in the hippocampus. *J. Neurosci.* 22:5525–5535.
11. Gillespie, D. T. 1992. A rigorous derivation of the chemical master equation. *Physica A.* 188:404–425.
12. Bortz, A. A., M. H. Kalos, and J. L. Lebowitz. 1975. A new algorithm for Monte Carlo simulation of Ising spin systems. *J. Comput. Phys.* 17: 10–18.
13. Fichthorn, K. A., and W. H. Weinberg. 1991. Theoretical foundations of dynamical Monte Carlo simulations. *J. Chem. Phys.* 95:1090–1096.
14. Schuhmeier, R. P., B. Dietze, F. Ursu, F. Lehmann-Horn, and W. Melzer. 2003. Voltage-activated calcium signals in myotubes loaded with high concentrations of EGTA. *Biophys. J.* 84:1065–1078.
15. Bhalla, U. S., and R. Iyengar. 1999. Emergent properties of networks of biological signaling pathways. *Science.* 283:381–387.
16. Kim, S. A., K. G. Heinze, M. N. Waxham, and P. Schwille. 2003. Intracellular calmodulin availability accessed with two-photon cross-correlation. *Proc. Natl. Acad. Sci. USA.* 101:105–110.
17. Shaevitz, J. W., S. M. Block, and M. J. Schnitzer. 2005. Statistical kinetics of macromolecular dynamics. *Biophys. J.* 89:2277–2285.
18. Colquhoun, D., and F. J. Sigworth. 1983. Fitting and statistical analysis of single-channel records. *In* Single-Channel Recordings. B. Sakman and E. Neher, editors. Plenum, New York.
19. Milescu, L. S., G. Akk, and F. Sachs. 2005. Maximum likelihood estimation of ion channel kinetics from macroscopic currents. *Biophys. J.* 88: 2494–2515.
20. Shnitzer, M. J., and S. M. Block. 1995. Statistical kinetics of processive enzymes. *Cold Spring Harb. Symp. Quant. Biol.* 60:793–802.

21. Harrison, P. G., and W. J. Knottenbelt. 2002. Passage time distributions in large Markov models. *ACM SIGMETRICS Perform. Eval. Rev.* 30:77–85.

22. Harris, K. M., and J. K. Stevens. 1989. Dendritic spines of CA1 pyramidal cells in the rat hippocampus: serial electron microscopy with reference to their biophysical characteristics. *J. Neurosci.* 9:2982–2997.

23. Sabatini, B. L., T. G. Oertner, and K. Svoboda. 2002. The life cycle of Ca^{2+} ions in dendritic spines. *Neuron.* 33:439–452.

24. Zhabotinsky, A. M., R. N. Camp, I. P. Epstein, and J. E. Lisman. 2006. Role of the neurogranin concentrated in spine in the induction of long-term potentiation. *J. Neurosci.* 26:7337–7347.

25. Quintana, A. R., D. Wang, J. E. Forbes, and N. M. Waxham. 2005. Kinetics of calmodulin binding to calcineurin. *Biochem. Biophys. Res. Commun.* 334:674–680.

26. Hanson, P. I., T. Meyer, L. Stryer, and H. Schulman. 1994. Dual role of calmodulin in autophosphorylation of multifunctional CaM kinase may underlie decoding of calcium signals. *Neuron.* 12:943–956.

27. Berridge, M. L. 2006. Calcium microdomains: organization and function. *Cell Calcium.* 40:405–412.

28. Andrews, S. S., and D. Bray. 2004. Stochastic simulation of chemical reactions with spatial resolution and single molecule detail. *Phys. Biol.* 1:137–151.

29. Franks, K. M., and T. J. Sejnowski. 2002. Complexity of calcium signaling in synaptic spines. *Bioessays.* 24:1130–1144.

30. Kubota, Y., T. R. Gaertner, J. A. Putkey, and N. M. Waxham. 2005. A novel Monte Carlo simulation for molecular interaction and diffusion in postsynaptic spines. *Neurocomputing.* 65–66:595–602.

31. Gerendasy, D. 1999. Homeostatic tuning of Ca^{2+} signal transduction by members of the calpacitin protein family. *J. Neurosci. Res.* 58:107–119.